

# Atomistic modeling of the reordering process of $\gamma'$ disordered particles in Ni–Al alloys



Enrique Martínez <sup>a,\*</sup>, Frédéric Soisson <sup>b</sup>, Alfredo Caro <sup>a</sup>, Blas P. Uberuaga <sup>a</sup>

<sup>a</sup> Material Science and Technology Division, MST-8, Los Alamos National Laboratory, Los Alamos, 87545 NM, USA

<sup>b</sup> DEN-Service de Recherches de Métallurgie Physique, CEA, Université Paris-Saclay, F-91191 Gif-sur-Yvette, France

## ARTICLE INFO

### Article history:

Received 11 March 2016

Received in revised form

7 June 2016

Accepted 8 June 2016

Available online 10 June 2016

### Keywords:

Segregation

Diffusion

Irradiation

## ABSTRACT

Ni-based alloys are used in nuclear applications, including as a window material at isotope production facilities, withstanding high fluxes of different energetic particles like protons. Irradiation disorders the  $\gamma'$  precipitates that in large extent confer the mechanical properties characterizing these materials. Upon disordering, the  $\gamma'$  phase transforms into oversaturated  $\gamma$ , degrading the materials properties. Experimentally it is observed that disordering might take place at fairly low irradiation doses. Once the particles are disordered, a competition between dissolution, due to strong concentration gradients in an oversaturated solid solution, and reordering appears. Here, we examine this competition in a model Ni–Al alloy under thermal conditions for different precipitates sizes and temperatures. We observe Al interdiffusion from the supersaturated particle to the matrix. Also, stochasticity appears as an important factor in to where precipitates locate. Stress relaxation seems to modify the precipitation process, with a stronger interface effect compared to rigid lattice simulations.

© 2016 Elsevier B.V. All rights reserved.

## 1. Introduction

In Ni-based alloys, the formation of L1<sub>2</sub>-ordered intermetallic  $\gamma'$  precipitates in a disordered  $\gamma$  matrix confers excellent mechanical properties to the system even at high temperature, such as high strength, with a weak dependence of the yield point with temperature, and a remarkable creep resistance. These properties make these materials ideal candidates for applications requiring high strength and fatigue resistance up to elevated temperatures, for instance, in turbine blades and discs in turboengines, and more recently, in power plants heat exchangers [1–3]. In nuclear environments, nickel-based alloys are used in vessel penetrations and steam generators due to their good corrosion properties [4]. These alloys are also used as proton beam windows [5,6] in proton accelerator facilities, subjected to stress-induced from differential pressure and thermal volume heating, and irradiation damage induced by primary protons and secondary neutrons.

Order-disorder transitions in Ni-based superalloys have been extensively studied in the literature [7,8]. Under irradiation, there is a competition between the disordering tendency induced by the

incoming energetic particles and the thermodynamic driving force restoring equilibrium [9–16]. It has been experimentally observed that the  $\gamma'$  precipitates disorder at much lower doses than they dissolve [17]. In Ni–Al alloys, when the particles disorder they become Al supersaturated  $\gamma$  phase. The relative free energy of the  $\gamma$  and  $\gamma'$  phases will determine the thermodynamic driving forces for reordering and dissolution. The reordering tendency, due to an enthalpic factor, will compete with the entropic contribution tending to homogenize the solid-solution phase. The different kinetics of each process will determine the final microstructure. This competition is the focus of this work.

Previous modeling efforts of the order-disorder process used either molecular dynamics (MD) [18–21] or rigid-lattice kinetic Monte Carlo (LKMC) [14] approaches. MD is limited in the achievable simulated time and, therefore, has focused on the early stages of precipitation and the disordering due to incident energetic particles with no recovery. As for the LKMC, it uses the assumption of infrequent events to accelerate the simulations, reaching longer times compared to MD. However, the evolution of the stresses in the sample is not considered, which might lead to deviations in the ordering pathways.

Experimental and modeling studies have also been devoted to the analysis of the properties of the order-disorder interphases [22–25]. They studied how the order parameter and the

\* Corresponding author.

E-mail address: [enrique@lanl.gov](mailto:enrique@lanl.gov) (E. Martínez).

composition change across the interphase and how the interphase free energy varies with orientation, which has implications in the ordering process.

Here, we use a kinetic Monte Carlo algorithm with full atomic relaxations to take into account the elastic energy to study how vacancy migration induces reordering in a system with a disordered  $\gamma'$  precipitate, depending on temperature and the precipitate radius.

### 1.1. Methodology

Fig. 1 shows the initial atomic configuration, with a spherical precipitate embedded in a disordered  $\gamma$  matrix. The figure also shows the total Al radial distribution for particles of 2.5 and 3.2 nm in radius. The Al content has been chosen to comply with the phase boundaries as described by the Embedded Atom Method (EAM) interatomic potential used in this study [22], which closely reproduces the experimental values (at 600 K,  $x_{Al}^{\gamma'} = 0.135$  and  $x_{Al}^{\gamma} = 0.24$ ; at 900 K,  $x_{Al}^{\gamma'} = 0.145$  and  $x_{Al}^{\gamma} = 0.22$ ; and at 1200 K,  $x_{Al}^{\gamma'} = 0.16$  and  $x_{Al}^{\gamma} = 0.213$ ). The ratio  $R/L$  (where  $R$  is the particle radius and  $L$  the box edge dimension) has been conserved in all simulations with a value of  $1/3$ , and we have studied particles with radius 2.5 and 3.2 nm [34]. We expect this ratio to be sufficient to avoid size effects as the stress field around a spherical inclusion decays as  $1/r^3$ . A vacancy was generated by removing an atom randomly.

In the Monte Carlo scheme, the vacancy migration rates ( $\Gamma_j$ ) were computed using Glauber dynamics

$$\Gamma_j = \frac{x_j}{1 + x_j}; \quad x_j = \exp(-\Delta E_j/kT) \quad (1)$$

where  $\Delta E_j$  is the change in energy between the final and initial configurations. The total pressure is relaxed to zero every 100 Monte Carlo steps to take into account the internal strain fields due to the lattice mismatch, and periodic boundary conditions were applied in every dimension. Once the rates were computed, the traditional BKL algorithm [26] was used to study the evolution of the microstructure under different conditions. This algorithm does

not accurately capture the dynamics of the process, but elucidates the most important effects in the competition between ordering and interdiffusion. In particular, because prefactors and barriers for each rate are not calculated, the time scale is not representative of the experiment, but the trajectories should be reasonable. To support this argument we have simulated the system kinetics at 600 K for the disordered 2.5 nm particle calculating the migration barrier using the nudged elastic band (NEB) method [27] at every step, also allowing for atomic relaxations. The rates are subsequently calculated according to harmonic transition state theory,  $\Gamma_j^{NEB} = \nu_0 \exp[-E^m/k_B T]$ , where  $\nu_0$  is the attempt frequency taken as the Debye frequency for each element,  $E^m$  is the vacancy migration energy as calculated using NEB,  $k_B$  is the Boltzmann constant and  $T$  the temperature. A full description of the algorithm can be found elsewhere [28]. Fig. 2 shows the evolution of the energy per atom of the system (solid lines) both using the full off-lattice KMC with NEB (hereafter referred to as OLKMC) and the Glauber dynamics with an effective jump frequency of  $1.8 \cdot 10^{-5} \text{ s}^{-1}$ , that, when multiplied by the number of steps, gives an estimate of the simulated time. The

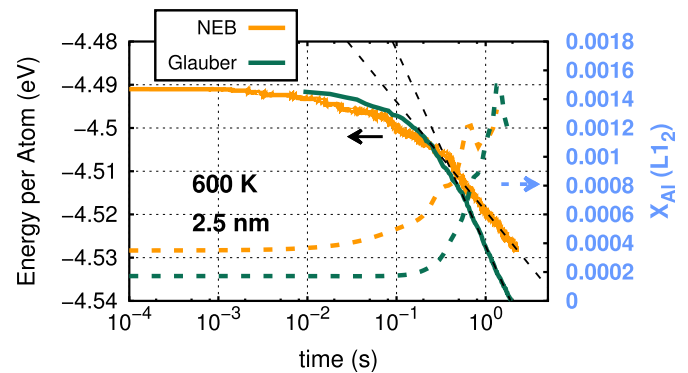


Fig. 2. Total energy per atom (solid lines) and fraction of Al in the  $L_{12}$  structure ( $X_{Al}(L_{12})$ , dashed lines) for a system with a disordered  $\gamma'$  particle of radius 2.5 nm comparing the evolution as given by the Glauber dynamics with an effective jump frequency of  $1.8 \cdot 10^{-5} \text{ s}^{-1}$  and the full off-lattice KMC calculating the migration barriers on-the-fly using NEB as described in Ref. [28]. The dashed black lines show the asymptotic behavior of the energy, as fitted to a  $E = a + \log(t^{-b})$  expression.

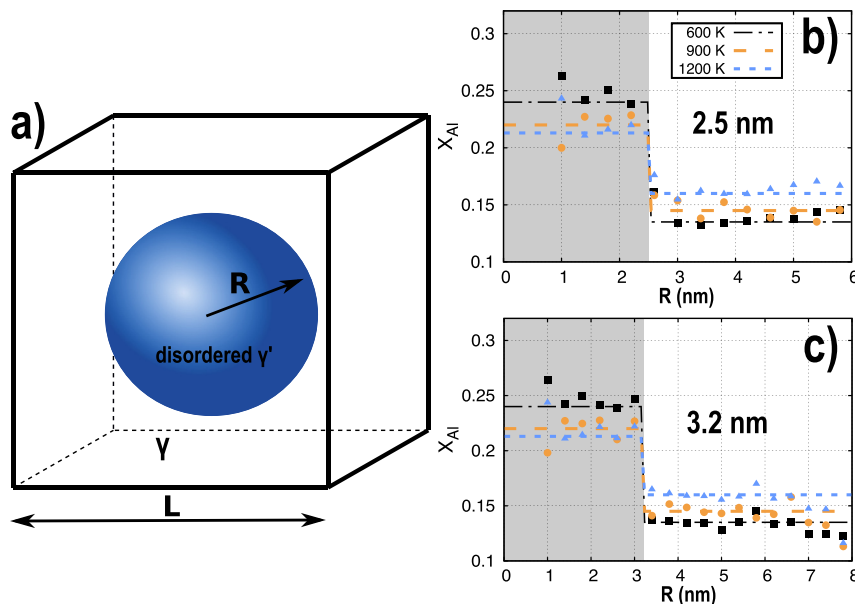


Fig. 1. a) Simulation setup and b)-c) Al spatial concentration distribution  $X_{Al}$  at different temperatures for a disordered  $\gamma'$  precipitate with  $R = 2.5$  and  $3.2$  nm, respectively, as a function of the distance from the center of the precipitate.

computational burden of the on-the-fly algorithm is between one and two orders of magnitude higher than the Glauber dynamics. The asymptotic behavior in both cases has been fitted to a expression of the form  $E = a + \log(t^{-b})$ , where  $t$  is the simulated time. The exponent  $b$  for the simulations using the OLKMC algorithm results in  $b = 0.011$ , while for the case of the Glauber dynamics became  $b = 0.019$ , with the same  $a = -4.52$ . Also shown in the figure is the evolution of the atomic fraction of Al in the  $L_{12}$  structure (color dashed lines), which, for the Glauber dynamics, indeed shows a similar tendency compared to the more accurate OLKMC algorithm. Thus, the Glauber dynamics do reproduce the qualitative behavior seen in the more accurate but more computationally expensive OLKMC simulations.

## 2. Results

### 2.1. Vacancy site energy

Fig. 3 shows the vacancy site energy defined as  $E_V^f = E[V] - (N_{Al}\mu_{Al} + N_{Ni}\mu_{Ni})$ , where  $E[V]$  is the energy of the relaxed system with one vacancy,  $N_{Al}$  and  $N_{Ni}$  are the number of Al and Ni atoms and  $\mu_X$  is the chemical potential of each species taken as the cohesive energy of the ground state crystal (single-element FCC for each). We show the results for a particle size of 2.5 nm in radius with a composition of each phase given by the boundaries of the two phase region in the phase diagram at 600 K; the behavior in the 3.2 nm case is similar. Fig. 3(a) displays the vacancy site energy of the initial system placing a vacancy in every atomic site when the  $\gamma'$  particle is fully disordered. Fig. 3(b) shows the energy of a system when the  $\gamma'$  particle is fully ordered and Fig. 3(c) presents the vacancy site energy after the sample was annealed with the Monte Carlo to  $5 \cdot 10^6$  steps. Inside the disordered particle there are Ni and Al sites with similar vacancy site energy (Fig. 3(a)), while in the matrix the vacancy seems to prefer Ni sites. For a fully ordered particle the vacancy tends to sit in Ni sites both inside and outside the particle (Fig. 3(b)). After the sample has been annealed, we observe that the vacancy site energy is fairly constant along the sample, with a preference to be in the Ni sites. The fact that outside the particle the results are not similar to the fully disordered case indicates that a certain degree of order has developed in the  $\gamma$  matrix also.

### 2.2. Microstructure evolution

Using the Glauber dynamics algorithm, we have performed five independent simulations, up to  $10^5$  Monte Carlo steps, for two systems with particle radii equal to 2.5 and 3.2 nm and three different temperatures, 600, 900 and 1200 K. These particle radii, at this supersaturations, are all above the critical nucleation radius for a  $\gamma'$  precipitate to be stable, as we shall see in Section 4, according to the interatomic potential used in the simulations. The results are shown in Fig. 4 where the average of the atomic fraction of Al atoms in the  $L_{12}$  structure and the standard error are shown. Al atoms were defined to be in an  $L_{12}$  structure when they are surrounded by 12 Ni atoms as first-nearest neighbors and 6 Al atoms as second-nearest neighbors, and the centro-symmetry parameter of the later is lower than 0.1. In the case of the smaller particle, 2.5 nm, (Fig. 4(a)), we observe that the initial stages of ordering take place in an outer shell of the particle, and not at its center. The amount of ordered Al increases at lower temperatures. As temperature increases, we notice a shift in the maximum of the fraction of Al in  $L_{12}$  structure towards the center of the particle.

For the larger particle tested in this study ( $R = 3.2$  nm), the ordering process seems to follow the same trend inside the particle with less influence from the interface, as shown in Fig. 4(b). Still, at lower temperatures, the observed maximum of the fraction of Al atoms in the  $L_{12}$  structure resides in a spherical layer between the center of the particle and the interface. This trend seems to diminish with temperature, with a higher fraction of  $L_{12}$  structure closer to the center of the disordered particle. For both sizes the degree of order decreases with increasing temperatures.

We have subsequently continue one out of the five independent simulations up to a total number of  $5 \cdot 10^6$  Monte Carlo steps in order to identify where the  $\gamma'$  precipitates finally grow. The distribution of Al fraction in  $L_{12}$  structure  $N_{Al}(L_{12})/N_{Al}$  at this stage is plotted in Fig. 5. The distribution in the interior of the small particles still peaks (except at 1200 K) in an intermediate shell and not at the center of the particle, although it has shifted towards the center compared to the distribution after  $10^5$  Monte Carlo steps. At

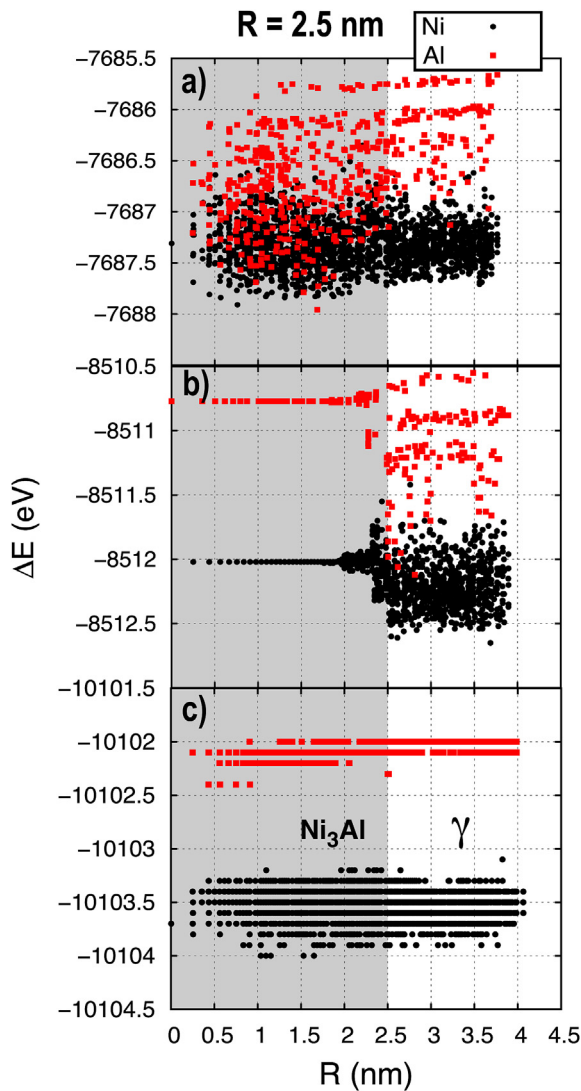


**Fig. 3.** Vacancy site energy for systems with a particle of 2.5 nm in radius for a) a fully disorder system with local concentration representative of the two phases; b) a perfectly ordered  $\gamma'$  particle and c) an annealed sample after  $5 \cdot 10^6$  Monte Carlo steps at 600 K. The shaded area indicates the domain of the disordered  $\gamma'$  particle (the initial region for the annealed sample). Black points represent the formation energy of vacancies placed on Ni sites, while red is for vacancies placed on Al sites. (For interpretation of the references to colour in this figure legend, the reader is referred to the web version of this article.)

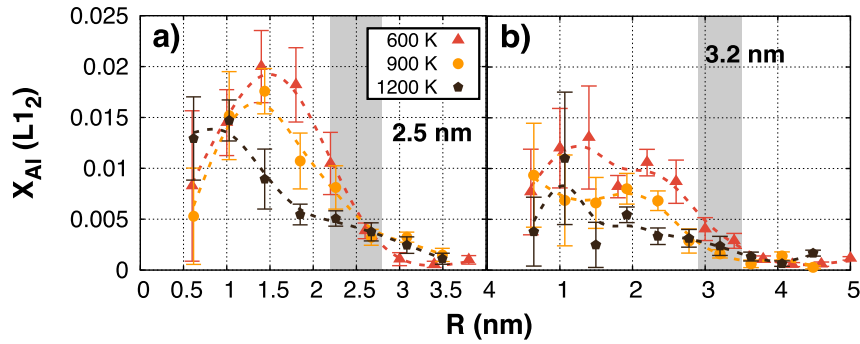


**Fig. 4.** Al fraction in  $L_{12}$  structure related to the total Al content  $N_{Al(L_{12})}/N_{Al}$  at 600, 900 and 1200 K for a disordered  $\gamma'$  particle of (a) 2.5 nm, and (b) 3.2 nm in radius after  $10^5$  Monte Carlo steps.

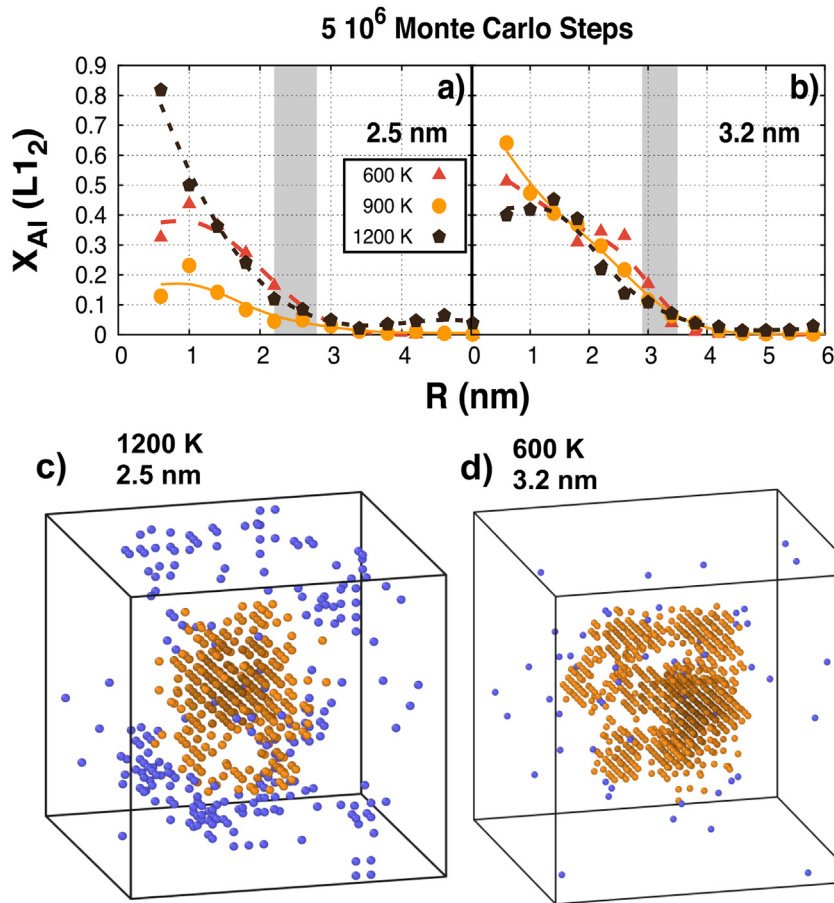


**Fig. 5.** Fraction of Al in the  $L_{12}$  structure related to the total Al content  $N_{Al(L_{12})}/N_{Al}$  for a) a particle radius of 2.5 nm; and b) a particle radius of 3.2 nm c-d) Al atoms in  $L_{12}$  structure after  $5 \cdot 10^6$  Monte Carlo steps (c) at 1200 K for an initial particle of 2.5 nm and (d) at 600 K for a particle of 2.5 nm. Brown particles highlight atoms with the  $L_{12}$  structure inside the initial supersaturated region while blue atoms are outside that region. The shaded area indicates the location of the interface. (For interpretation of the references to colour in this figure legend, the reader is referred to the web version of this article.)

1200 K the highest degree of ordering takes place preferentially at the center of the disordered region. We will analyze the origin of this trend in Section 4. For the larger particle, the effect of the interface is less pronounced, and the particle interior seems to be richer in  $L_{12}$  Al than the outer shells. The amount of Al in the  $L_{12}$  structure outside the initial disordered region is slightly larger (distances greater than 3.5 nm) with higher temperature, indicating a transfer of Al from the supersaturated region to the matrix. In the particle interior close to the interface, the trend is the opposite, with more  $Al(L_{12})$  at lower temperatures. This suggests

that the increase of Al in the matrix comes at the expense of the outer diameter of the precipitate region, further suggesting that the particle, when it finally reforms, may in fact be smaller than it was originally. Fig. 5(c) and (d) show the Al atoms in a  $L_{12}$  structure after  $5 \cdot 10^6$  Monte Carlo steps for a system at 1200 K with a 2.5 nm disordered  $\gamma'$  particle (Fig. 5(c)) and a sample at 600 K with a disordered precipitate of 3.2 nm (Fig. 5(d)). The atoms are colored according to their position: orange if they are inside the initial particle volume and blue if they are outside. For the larger particle at lower temperature we observe that most of the  $L_{12}$  structured Al



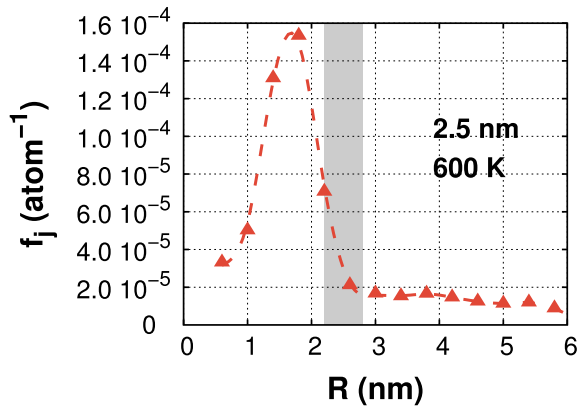


**Fig. 6.** Normalized number frequency that the vacancy spent in different spherical shells for a total run of 39,735 KMC steps giving a total time of 2.35 s, in a sample with an initial 2.5 nm disordered particle at 600 K. The shaded area indicates the position of the interface.

remains inside the original particle volume, whereas at high temperature for the smaller particle some of the ordered phase forms outside the original precipitate volume.

To better understand the kinetics that drive the reordering process, we have analyzed the vacancy evolution for the calculations performed using the OLKMC algorithm. The results are plotted in Fig. 6, where the fraction of exchanges performed by the vacancy in a concentric spherical shell normalized by the number of atoms in the shell is presented. The time interval analyzed goes up to 2.35 s. A clear peak is observed near the interface, where the vacancy resides for most of the exchanges. The presence of the vacancy near the interface region of the sample leads to two effects, an initially larger degree of order in an outer region of the particle, in agreement with Fig. 4(a), and a substantial Al interdiffusion toward the matrix. Fig. 7 shows the evolution of the vacancy migration energy as it exchanges with a Ni or an Al atom as obtained from the OLKMC. We have studied different initial conditions, obtained at different Monte Carlo steps using the Glauber dynamics algorithm. We have estimated the initial time for those samples using the  $1.8 \cdot 10^{-5}$  coefficient found above. We note that the migration barrier for a vacancy–Al exchange is lower than for a Ni hop, 0.77 eV versus 1.06 eV at the initial stages of the process. The estimated average evolves in time, increasing its values for both Ni and Al. From 1.9 to 2.7 s, the Ni barrier is still larger than the Al. Both barriers increased in this period, although Al did in a larger extent, with respect to the previous time interval ([0:0.14] s). Between 18 and 20 s we observe a crossover, with the Al barrier becoming larger than the Ni. This last one did not significantly change with respect to the previous interval. For the latest period, with the

larger degree of order, the Al migration barrier is significantly higher than the Ni in about 0.17 eV. This evolution of the barriers, in combination with Fig. 3, gives an overall picture of the process: Al preferentially exchanges with the vacancy for a low degree of order, while at higher degree of order, Ni has a larger probability to hop into the unoccupied site.

### 3. Discussion

These calculations were performed for systems with composition inside the miscibility gap, *i.e.*, the tendency for the system to order is larger than the thermodynamic driving force for the system to homogenize in a solid solution. Therefore, the kinetic competition between reordering and dissolution will determine the final microstructure. We have seen that the amount of Al interdiffusion depends on the particle radius and the temperature and that for small particles and high temperatures the precipitation process might lead to L1<sub>2</sub> particles outside the original disordered  $\gamma'$  precipitate.

To further clarify the interdiffusion process, we show in Fig. 8 the initial and final fraction of Al depending on the distance to the particle center for a 2.5 nm radius particle (Fig. 8(a)) and a 3.2 nm radius particle (Fig. 8(b)) as a function of temperature. It is clear that the Al diffuses from the supersaturated particle to the matrix for both cases and for all the temperatures studied. The effect is more pronounced for the smaller particle.

This interdiffusion reduces the supersaturation close to the interface, which displaces the driving force for precipitation inwards into the disordered particle. Since the vacancy tends to stay close to the interface, the first stages of precipitation occur in a spherical shell in which the supersaturation is important and the vacancy is available to order the system. To analyze the entropic effect due to the particle disorder, we run simulations with the same configuration at 600 K although the particle was initially ordered in a L1<sub>2</sub> structure. The results after  $10^6$  Monte Carlo steps are shown in Fig. 9. We observe that the variation in the total Al distribution is minimal, what suggests that the disorder induces a non-negligible thermodynamic force for homogenization that leads to Al interdiffusion towards the matrix.

The fact that some interdiffusion takes place before reordering happens leads to the possibility of the full dissolution of small particles increasing the supersaturation of the matrix. This extra Al might diffuse to larger particles to form bigger precipitates which would contribute to coarsening. As new radiation damage events continue to disorder precipitates, smaller precipitates will completely dissolve. This process might lead to the formation of metastable structures like the ones described in Ref. [29]. Further, there may be a maximum size for ordered precipitates as the disordering–ordering cycle tends to deplete Al at the interfacial

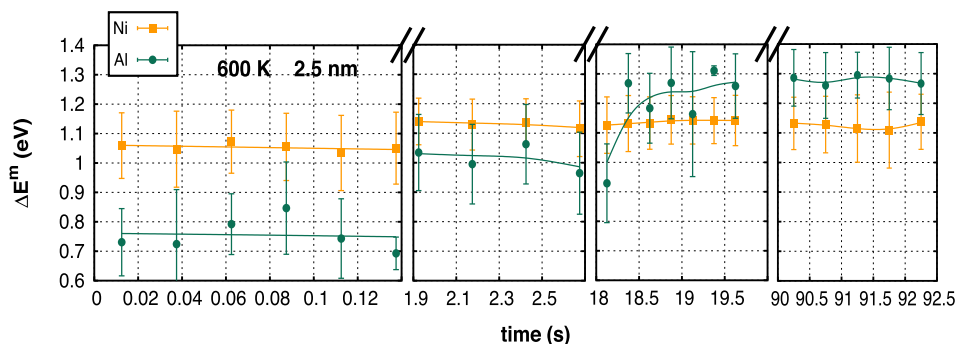


**Fig. 7.** Evolution of the average of the vacancy migration energy as it exchanges with Ni or Al and its standard deviation as obtained with the OLKMC algorithm using NEB.

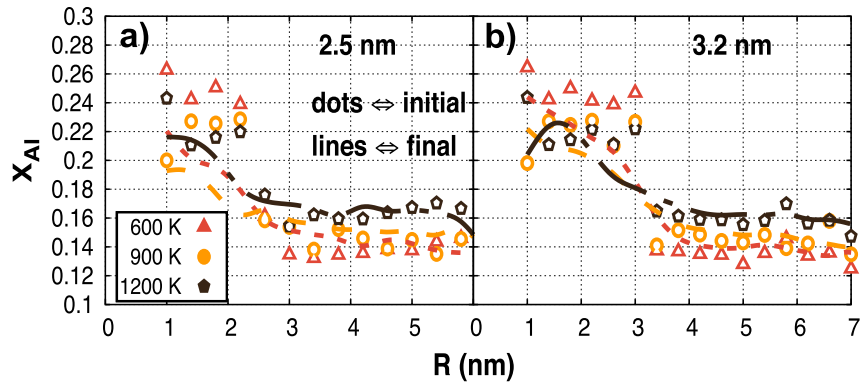


Fig. 8. Initial and final fraction of Al after  $5 \cdot 10^6$  Monte Carlo steps for a) a particle radius of 2.5 nm; and b) a particle radius of 3.2 nm.

region, implying particles cannot grow without bound. This is similar to the behavior observed for Xe bubbles in  $\text{UO}_2$  [30].

### 3.1. Effect of the initial configuration

We have studied the effect of the initial configuration on the ordering tendency for samples with a 2.5 nm radius disordered particles. The initial structures were created with the same target concentration for the particle and the matrix, but with different random seeds for the Al distribution, thus Al locates at different sites. The results after  $5 \cdot 10^6$  Monte Carlo steps are shown in Fig. 10. At 600 K and 900 K, the change in the initial configuration has a moderate effect in the final distribution of Al in  $L_{12}$  structure. On the other hand, at 1200 K the distribution of ordered Al strongly depends on the initial conditions. At high temperatures the ordering tendency decreases, with a higher entropic component, which makes the propensity of nucleation smaller. This leads to further atomic transport and a more significant stochasticity of the precipitate microstructure.

### 3.2. Effect of the interface curvature

To probe the effect of interfacial curvature (Gibbs-Thompson effect) in the ordering process, we have simulated the evolution in samples with two planar interfaces for the same conditions as above: temperatures of 600, 900 and 1200 K with concentrations complying with the phase diagram. The results for the Al atomic fraction in a  $L_{12}$  structure are presented in Fig. 11. The results show a snapshot of the configuration after  $2 \cdot 10^5$  MC steps. There is a

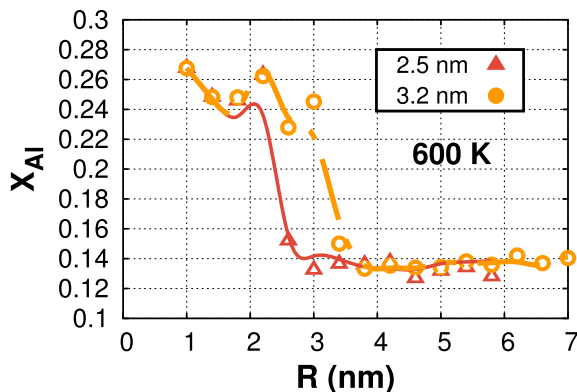


Fig. 9. Initial (points) and final (lines) fraction of Al after  $10^6$  Monte Carlo steps for an ordered particle with 2.5 nm and 3.2 nm radius.

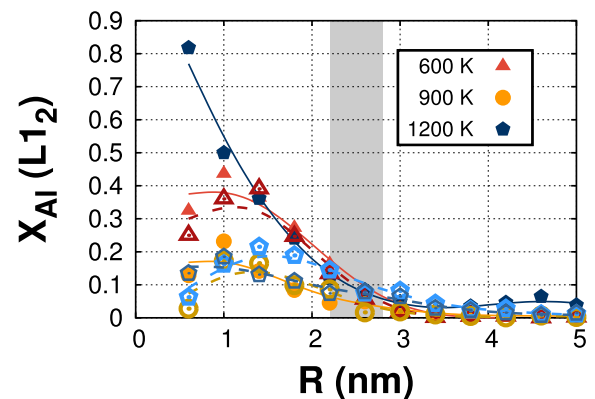


Fig. 10. Fraction of Al in  $L_{12}$  structure related to the total Al content  $N_{Al}(L_{12})/N_{Al}$  after  $5 \cdot 10^6$  Monte Carlo steps for a system with initial disordered  $\gamma'$  particle of 2.5 nm. Two different initial configurations were tested at 600 K (red triangles) and 900 K (yellow circles), and three configuration were analyzed at 1200 K (blue pentagons). (For interpretation of the references to colour in this figure legend, the reader is referred to the web version of this article.)

substantial interface effect, more pronounce at low temperature, with a larger fraction of  $L_{12}$  structure occurring preferentially near one of the interfaces, though the distributions vary significantly over the length of the supersaturated region. As with the spherical particles, there is also a tendency for  $L_{12}$  to form in the original matrix region, indicating a net transport of Al from the supersaturated particle to the matrix.

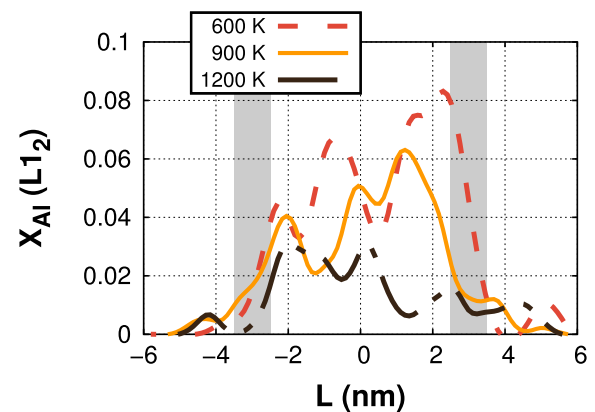
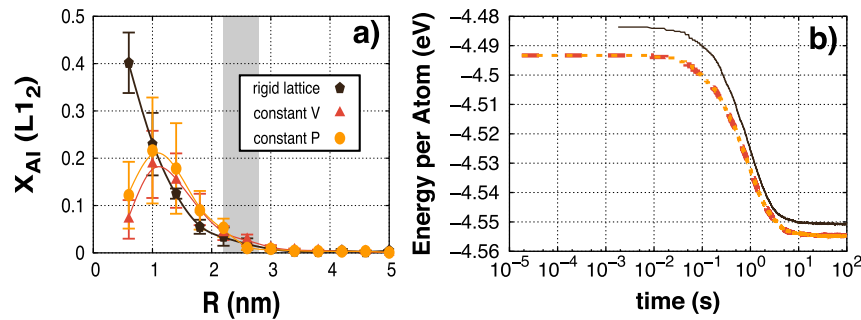


Fig. 11. Fraction of Al in the  $L_{12}$  structure related to the total Al content  $N_{Al}(L_{12})/N_{Al}$  for a  $\gamma - \gamma'_{dis}$  with two interfaces (shaded area) after  $2 \cdot 10^5$  Monte Carlo steps at different temperatures.



**Fig. 12.** Fraction of Al in L<sub>12</sub> structure related to the total Al content  $N_{Al}(L_{12})/N_{Al}$  and (b) energy per atom after  $5 \cdot 10^6$  Monte Carlo steps for a system with initial disordered  $\gamma'$  particle of 2.5 nm at 900 K for different boundary conditions, a rigid lattice, constant volume and constant pressure at 0 MPa.

### 3.3. Effect of the stress relaxation

Our Monte Carlo algorithm allows for atomic relaxations, being able to relax the stress in the sample as the microstructure evolves. To identify how allowing for these relaxations influences the final result of the simulation, we have simulated three different conditions – a rigid lattice, a constant volume and a constant pressure approach, relaxing the atomic configuration every 100 Monte Carlo steps – with the same initial configuration and run for  $5 \cdot 10^6$  steps with different random seeds. Three different simulations were run with the rigid lattice algorithm and two at constant V and constant pressure. The results are shown in Fig. 12. Substantial difference is observed between the unrelaxed structure (rigid lattice) and the relaxed system, mostly at the particle inner core. The rigid lattice seems to over-estimate the amount of precipitation at the center of the particle, with the maximum corresponding to the center of the particle interior. On the other hand, when the stress is relaxed, there seems to be a larger effect of the presence of the interface, with greater ordering closer to it than in the rigid lattice approach, and lower at the particle center. It is hard to draw a clear conclusion on the effect of relaxation, since, as we mentioned above, stochasticity seems to play a fundamental role in the process.

The evolution of the energy per atom in the different cases studied is also shown in Fig. 12(b). The atomic relaxations lead to an overall decrease in the energy of the system. Moreover, a slightly different exponent in the energy evolution is found. No significant variation is observed in the energy evolution between the simulations at constant volume and constant pressure.

### 3.4. Experimental insight

Recent experimental work on Rene N4 [31] and Inconel X-750 [32,33] superalloys agrees with older results [13,17] in that, at temperatures below  $\sim 700$  K, the  $\gamma'$  precipitates first disorder at lower dpa and finally dissolve at much larger dpa. To the best of our knowledge there is no experimental evidence of the role of elastic strain in the competition between reordering and disordering in Ni alloys under irradiation. The evolution of a disordered particle does not have to match the growth mechanism of ordered precipitates, and the role of the interface in the process might be different. It would be useful to perform experimental tests in NiAl and NiAlCr (for example), with high and low lattice mismatch, respectively, under irradiation, to observe the evolution of the disordered precipitates and compare under exactly the same conditions the reordering kinetics. It would be important in this case to rule out any effect due to chemistry to focus on the influence of strain.

It is also worth mentioning that our calculations were performed at a fixed defect concentration independent of temperature, there was always only one vacancy in the simulation box. The

presence of a larger defect concentration or different types of defects would undoubtedly modify the process kinetics. However, in this work we focused on the basic mechanisms for reordering under as close to thermal conditions as possible.

## 4. Conclusions

We have studied the reordering process of a disordered  $\gamma'$  particle in the context of Ni-Al superalloys under irradiation. We have used a Monte Carlo algorithm with full atomic relaxations to analyze the system evolution. Close to the interface the tendency to homogenization (entropic driving force) is larger than the ordering tendency, which diffuses the width of the interface, from sharp to a broader structure. This leads to Al interdiffusion from the particle to the matrix, depleting the interface. We also note that vacancies are more likely to be close to the interface, as needed for the interdiffusion. This leads to the initial stages of precipitation to happen preferentially near the interface, in an outer shell of the disordered particle.

The vacancy migration barrier depends on the jumping atom and the environment. At the initial stages, the Al barrier is lower than the Ni. As the system evolves the migration barrier for the vacancy to jump into an Al increases, while the exchange with a Ni atom remains fairly constant. This leads to a crossover for a certain degree of order at which the vacancy-Al exchange has a larger barrier than the exchange with Ni, and, subsequently, the vacancy preferentially remains in the Ni sublattice.

The effect of the initial configuration seems to be more important at higher temperatures, but the variation in the distribution of Al L<sub>12</sub> structure might change considerably, which suggest that stochasticity plays an important role in the precipitation process. Also worth noting is the fact that the results indicate that the system relaxation seems to shift the maximum degree of ordering from the center of the particle to an outer shell closer to the interface, which seems to be the result of a competition between the system relaxation and the ordering tendency.

## Acknowledgements

The authors gratefully acknowledge the support of the US Department of Energy (DOE) through the LANL/LDRD Program for this work. This research used resources provided by the LANL Institutional Computing Program. LANL, an affirmative action/equal opportunity employer, is operated by Los Alamos National Security, LLC, for the National Nuclear Security Administration of the U.S. DOE under contract DE-AC52-06NA25396.

## References

- [1] J.H. Westbrook, R.L. Fleischer, *Structural Applications of Intermetallic Compounds*, Wiley, New York, 2000.
- [2] D. Shah, E. Lee, *Intermetallic Compounds*, John Wiley and Sons, Chichester, 2002.
- [3] K.J. Hemker, W.D. Nix, *Structural Intermetallics*, TMS, Warrendale, 1997.
- [4] S.J. Zinkle, G.S. Was, Materials challenges in nuclear energy, *Acta Mater.* 61 (2013) 735–758.
- [5] S. Meigo, M. Ooi, M. Harada, H. Kinoshita, A. Akutsu, Radiation damage and lifetime estimation of the proton beam window at the japan spallation neutron source, *J. Nucl. Mater.* 450 (2014) 141–146.
- [6] H.T. Bach, O. Anderoglu, T.A. Saleh, T.J. Romero, C.T. Kelsey, E.R. Olivas, B.H. Sencer, P.O. Dickerson, M.A. Connors, K.D. John, S.A. Maloy, Proton irradiation damage of an annealed alloy 718 beam window, *J. Nucl. Mater.* 459 (2015) 103–113.
- [7] R.C. Reed, *The Superalloys: Fundamentals and Applications*, Cambridge University Press, 2006.
- [8] A.J. Ardell, V. Ozolins, Trans-interface diffusion-controlled coarsening, *Nat. Mater.* 4 (2005) 309–316.
- [9] D.I. Potter, H.A. Hoff, Irradiation effects on precipitation in  $\gamma$ – $\gamma'$  nial alloys, *Acta Metall.* 24 (1976) 1155–1164.
- [10] D. Potter, D. Ryding, *J. Nucl. Mater.* 71 (1977) 14–24.
- [11] D. Potter, P. Okamoto, H. Wiedersich, J. Wallace, A. McCormick, *Acta Metall.* 27 (1979) 1175–1185.
- [12] F. Bourdeau, E. Camus, C. Abromeit, H. Wollenberger, Disorder and dissolution of  $\gamma'$  precipitates under ion irradiation, *Phys. Rev. B* 50 (1994) 16205.
- [13] E. Camus, C. Abromeit, F. Bourdeau, N. Wanderka, H. Wollenberger, Evolution of long-range order and composition for radiation-induced precipitate dissolution, *Phys. Rev. B* 54 (1996) 3142.
- [14] G. Martin, P. Bellon, *Solid State Phys.* 50 (1997) 189–331.
- [15] C. Abromeit, E. Camus, S. Matsumura, Modelling of dissolution profiles of ordered particles under irradiation, *J. Nucl. Mater.* 271 (1999) 246.
- [16] M. Nastasi, H.H. Johnson, J.W. Mayer, J.M. Williams, Stability and formation of  $\text{NiAl}_3$  under irradiation, *J. Mater. Res.* 1 (1986) 268–274.
- [17] S. Muller, C. Abromeit, S. Matsumura, N. Wanderka, H. Wollenberger, Disordering kinetics of  $\text{Ni}_3\text{Al}$  under ion irradiation, *J. Nucl. Mater.* 271–272 (1999) 241–245.
- [18] T. Diaz de la Rubia, A. Caro, M. Spaczer, Kinetics of radiation-induced disordering of a3b intermetallic compounds: a molecular-dynamics-simulation study, *Phys. Rev. B* 47 (1993) 11483.
- [19] M. Spaczer, A. Caro, M. Victoria, T. Diaz de la Rubia, Computer simulations of disordering and amorphization kinetics in intermetallic compounds, *Nucl. Inst. Meth. Phys. Res. B* 102 (1995) 81–85.
- [20] P. Oramus, C. Massobrio, M. Kozłowski, R. Kozubski, V. Pierron-Bohnes, M.C. Cadeville, W. Pfeiler, Ordering kinetics in  $\text{ni}_3\text{al}$  by molecular dynamics, *Comp. Mater. Sci.* 27 (2003) 186–190.
- [21] T. Lee, A. Caro, M.J. Demkowicz, Atomistic modeling of radiation-induced disordering and dissolution at a  $\text{Ni}/\text{Ni}_3\text{Al}$  interface, *J. Mater. Res.* 30 (2015) 1456–1463.
- [22] Y. Mishin, Atomistic modeling of the gamma and gamma' phases of the Ni–Al system, *Acta Mater.* 52 (2004) 1451–1467.
- [23] Y. Mishin, Calculation of the  $\gamma/\gamma'$  interface free energy in the Ni–Al system by the capillary fluctuation method, *Model. Simul. Mater. Sci. Eng.* 22 (2014) 045001.
- [24] R. Srinivasan, R. Banerjee, J.Y. Hwang, G.B. Viswanathan, J. Tiley, D.M. Dimiduk, H.L. Fraser, Atomic scale structure and chemical composition across order-disorder interfaces, *Phys. Rev. Lett.* 102 (2009) 086101.
- [25] Z. Mao, C. Booth-Morrison, E. Plotnikov, D.N. Seidman, Effects of temperature and ferromagnetism on the  $\gamma$ – $\text{Ni}/\gamma'$ – $\text{Ni}_3\text{Al}$  interfacial free energy from first principles calculations, *J. Mater. Sci.* 47 (2012) 7653–7659.
- [26] A.B. Bortz, M.H. Kalos, J.L. Lebowitz, A new algorithm for monte carlo simulation of ising spin systems, *J. Com. Phys.* 17 (1975) 10–18.
- [27] G. Henkelman, B.P. Uberuaga, H. Jonsson, A climbing image nudged elastic band method for finding saddle points and minimum energy paths, *J. Chem. Phys.* 113 (22) (2000) 9901–9904.
- [28] E. Martínez, A. Caro, Atomistic modeling of long-term evolution of twist boundaries under vacancy supersaturation, *Phys. Rev. B* 86 (2012) 214109.
- [29] R.A. Enrique, P. Bellon, Compositional patterning in systems driven by competing dynamics of different length scale, *Phys. Rev. Lett.* 84 (13) (2000) 2885–2888.
- [30] D. Schwen, R.S. Averback, Intragranular xe bubble population evolution in uo2: a first passage monte carlo simulation approach, *J. Nucl. Mater.* 402 (2010) 116–123.
- [31] C. Sun, et al., Microstructure, chemistry and mechanical properties of Ni-based superalloy Rene N4 under irradiation at room temperature, *Acta Mater.* 95 (2015) 357–365.
- [32] H.K. Zhang, Z. Yao, C. Judge, M. Griffiths, Microstructural evolution of CANDU spacer material Inconel X-750 under in situ ion irradiation, *J. Nucl. Mater.* 443 (2013) 49–58.
- [33] H.K. Zhang, Z. Yao, M.R. Daymond, M.A. Kirk, Elevated temperature irradiation damage in CANDU spacer material Inconel X-750, *J. Nucl. Mater.* 445 (2014) 227–234.
- [34] Particles with 1.8 nm radius were also studied although much noise was found to draw clear conclusions.